

Low energy cooling for Electron Ion Collider

A. Fedotov

December 2020

Electron-Ion Collider
Brookhaven National Laboratory

U.S. Department of Energy

USDOE Office of Science (SC), Nuclear Physics (NP) (SC-26)

Notice: This technical note has been authored by employees of Brookhaven Science Associates, LLC under Contract No. DE-SC0012704 with the U.S. Department of Energy. The publisher by accepting the technical note for publication acknowledges that the United States Government retains a non-exclusive, paid-up, irrevocable, world-wide license to publish or reproduce the published form of this technical note, or allow others to do so, for United States Government purposes.

DISCLAIMER

This report was prepared as an account of work sponsored by an agency of the United States Government. Neither the United States Government nor any agency thereof, nor any of their employees, nor any of their contractors, subcontractors, or their employees, makes any warranty, express or implied, or assumes any legal liability or responsibility for the accuracy, completeness, or any third party's use or the results of such use of any information, apparatus, product, or process disclosed, or represents that its use would not infringe privately owned rights. Reference herein to any specific commercial product, process, or service by trade name, trademark, manufacturer, or otherwise, does not necessarily constitute or imply its endorsement, recommendation, or favoring by the United States Government or any agency thereof or its contractors or subcontractors. The views and opinions of authors expressed herein do not necessarily state or reflect those of the United States Government or any agency thereof.

| | |
|--|-----------------------|
| EIC TECHNICAL NOTE | NUMBER |
| | EIC-HDR-TN-012 |
| AUTHORS: S. Benson, M. Bruker, A. V. Fedotov, X. Gu, C. Gulliford, J. Guo, A. Hutton, J. Kewisch, D. Kayran, V. Ptitsyn, R. Rimmer, T. Satogata, S. Seletskiy, A. Seryi, E. Wang, H. Wang, H. Zhang, Y. Zhang, and H. Zhao | DATE 12/10/2020 |
| Low-Energy Cooling for the Electron Ion Collider | |

Low-Energy Cooling for the Electron Ion Collider

S. Benson,^{1,*} M. Bruker,¹ A. V. Fedotov,^{2,†} X. Gu,² C. Gulliford,³ J. Guo,¹
A. Hutton,¹ J. Kewisch,² D. Kayran,² V. Ptitsyn,² R. Rimmer,¹ T. Satogata,¹
S. Seletskiy,² A. Seryi,¹ E. Wang,² H. Wang,¹ H. Zhang,¹ Y. Zhang,¹ and H. Zhao²

¹*Jefferson Lab, 12000 Jefferson Ave, Newport News, VA 23606, USA*

²*Brookhaven National Laboratory, Upton, NY 11973, USA*

³*Cornell University, Ithaca, NY 14853, USA*

(Dated: December 10, 2020)

I. INTRODUCTION

Luminosity parameters at the highest hadron energy in the Electron Ion Collider (EIC) [1] require a proton beam with a small vertical emittance. Such a small emittance can be obtained using the technique of electron cooling [2], by pre-cooling of the proton bunches at an injection energy of 23.8 GeV. After pre-cooling, the proton bunches are accelerated to the maximum energy for collisions. Once at the top energy, such proton bunches can be refilled frequently to maintain a high average luminosity [3], or, alternatively, cooling at the top energy could be provided with relaxed requirements of just counteracting the emittance growth due to Intra-Beam Scattering (IBS) and thus maintaining the luminosity close to its initial peak value. Presently, several schemes of cooling at the top energy of 275 GeV are being considered with the goal to maintain the initial proton beam parameters, thus relying on pre-cooling at the low energy to obtain such initial parameters of proton bunches.

For the lowest proton collision energy of 41 GeV in the EIC, there is a need for an electron cooler which counteracts the beam emittance growth due to IBS. This can be achieved by the same electron cooler which is used for cooling of protons at 23.8 GeV. In this case, we assume the electron cooler first pre-cools protons at an injection energy of 23.8 GeV and then, after acceleration, cools the 41 GeV protons, counteracting IBS and maintaining the beam emittances.

In this report, we summarize a feasibility study of an electron cooler that would be needed to cool protons at 23.8 GeV to obtain a small vertical emittance, as well as to counteract beam growth due to IBS for collisions at 41 GeV.

The traditional electron cooling system employed at a typical low-energy cooler is based on an electron beam generated with an electrostatic electron gun in DC operating

* felman@jlab.org

† fedotov@bnl.gov

mode, immersed in a longitudinal magnetic field. To cool protons at 23.8 and 41 GeV, electron beam energies of 13.0 and 22.3 MeV, respectively, are required. Due to the technical limitations of static high-voltage acceleration, these beam energies require RF acceleration of a pulsed electron beam. Electron cooling using RF-accelerated electron bunches was recently successfully commissioned in RHIC [4], allowing us to consider such an approach for EIC low-energy electron cooling.

II. CHOICE OF COOLING APPROACH

Most existing electron coolers use strong longitudinal magnetic fields in the cooling section. This field changes the collision kinetics significantly by limiting the transverse motion of the electrons. In the limit of a very strong magnetic field, the transverse degree of freedom does not take part in the energy exchange because collisions are adiabatically slow relative to the Larmor oscillations. As a result, the efficiency of electron cooling is determined mainly by the longitudinal velocity spread of the electrons. Such cooling is typically referred to as “magnetized cooling” [5, 6]. For high-energy applications, this approach becomes very technically demanding due to the need for a very long solenoid with extremely tight field tolerances, and due to the difficulty of preserving the magnetization of the electron beam during beam transport from the cathode to the cooler.

On the other hand, when the RMS velocity spread within the electron beam is comparable to the spread within the ion beam, electron cooling can be performed effectively without the help of a strong external magnetic field in the cooling section. Such cooling is referred to as “non-magnetized” cooling. This scheme does not preclude the use of a weak continuous external magnetic field, both to counteract focusing effects from the ions in the cooling section and to ensure the required overlap of the electron and ion beams. If the focusing field is present only in short segments of the cooling section, a non-magnetized beam may be used, as in LEReC [4]. If a continuous longitudinal field in the cooling section is used, the same magnetic flux must be present at the cathode, as in the case of the FNAL electron cooler [7].

Since it appears feasible to produce an electron beam with the required charge per bunch and with the required electron beam quality, as discussed in the following sections, an approach with a non-magnetized electron beam was selected. This significantly simplifies the cooler design.

With no magnetic field, the friction force on an ion inside a uniform-density electron gas with a velocity distribution function $f(v_e)$ is given by [5, 8]:

$$\vec{F} = -\frac{4\pi n_e e^4 Z^2}{m_e} \int L_C \frac{\vec{V}_i - \vec{v}_e}{|\vec{V}_i - \vec{v}_e|^3} f(v_e) d^3 v_e, \quad (1)$$

where Z is the ion charge number, e is the electron charge, n_e is the electron density, m_e is the electron mass, \vec{V}_i and \vec{v}_e are the ion and electron velocities, and $L_C = \ln(\rho_{\max}/\rho_{\min})$ is the Coulomb logarithm where ρ_{\max} and ρ_{\min} are the maximum and minimum impact parameters, respectively.

III. ELECTRON COOLER PARAMETERS FOR PRE-COOLING AT THE PROTON INJECTION ENERGY OF 23.8 GeV

As noted previously, the electron cooling time grows rapidly as a function of beam energy. This shortcoming of electron cooling might be partially mitigated by pre-cooling at low energy, where the cooling time is much shorter.

The goal of pre-cooling of protons at the injection energy is to obtain a small RMS normalized vertical emittance of 0.45 mm mrad. Cooling simulations have been performed to determine the electron beam parameters required to achieve such a vertical emittance on a time scale of 30–50 minutes. To determine the required electron bunch charge needed for cooling, an electron bunch with the same length and transverse beam sizes as those of the proton bunch was used initially, resulting in the charge requirement of 5 nC.

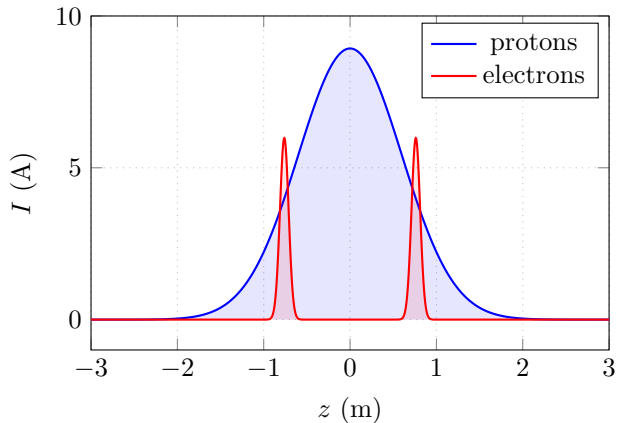


FIG. 1. Time structure of two electron bunches synchronized with a single proton bunch for cooling at 23.8 GeV.

At 23.8 GeV, the length of the proton bunches is 60 cm to 90 cm RMS depending on the RF voltage. Obtaining an electron bunch this long requires the use of very-low-frequency RF for acceleration or stretching the electron bunch after acceleration. Also, for a long electron bunch, the focusing caused by the proton space charge becomes significant, requiring the use of a weak continuous magnetic field in the cooling section

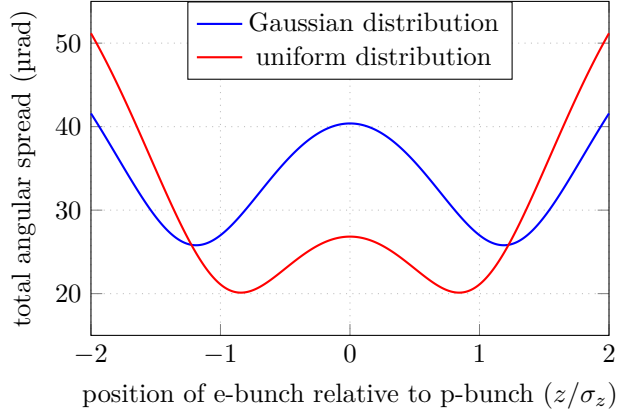


FIG. 2. Electron angles in the cooling section produced by beam emittance and proton space charge for cooling at 23.8 GeV for two possible electron bunch profiles.

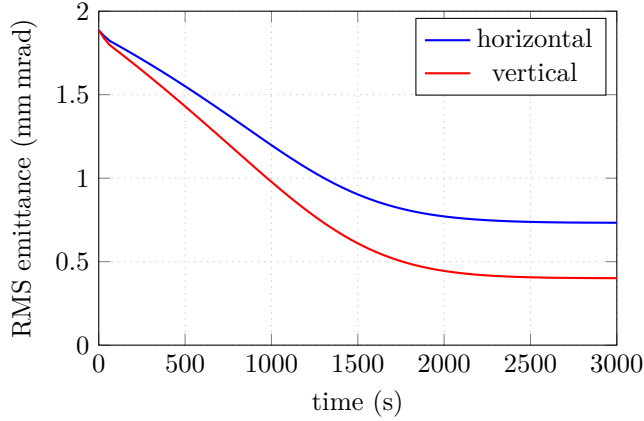


FIG. 3. RMS normalized emittance during cooling at 23.8 GeV using two electron bunches located at \pm one longitudinal RMS length of the proton bunch, with electron beam parameters from Table I.

in order to keep the angular spread of the electrons at the required level [11]. If one wants to use the same cooler to cool protons at 41 GeV where the proton bunches are short (7.5 cm RMS), a high-frequency RF linac is required.

If one employs short electron bunches with high peak current, one can choose temporal locations within the long proton bunch such that the contribution of transverse focusing from protons on the electron angles is not significant [12]. In such a case, no continuous magnetic field in the cooling section is required, thus allowing the use of

an electron beam without magnetization at the cathode. This significantly simplifies the technical design of the electron cooler.

The concept of cooling a very long ion bunch with short electron bunches was demonstrated in the LEReC cooler, where a frequency of 704 MHz is used for the electron accelerator. As many as 30 electron bunches in a so-called macro-bunch were synchronized with the ion bunches at a repetition rate of 9 MHz [9].

A 197 MHz RF linac allows us to put two electron bunches on a single proton bunch with 60 cm RMS length. Going to even higher frequencies of 394 MHz or 591 MHz allows us to put four or six electron bunches on a single proton bunch, respectively. Cooling simulations were performed for all these frequencies. The 197 MHz RF frequency of the linac—thus, an approach with two electron bunches per proton bunch—was chosen as shown in Fig. 1. Other choices of RF frequency could be considered during the design stage of the cooler.

In simulations, we assumed the total angular spread of the electrons in the cooling section to be $30 \mu\text{rad}$. The contributions to the angles in the cooling section from the electron beam emittance and the space charge of the proton beam are shown in Fig. 2. As can be seen from the results of cooling simulations with two electron bunches per proton bunch shown in Fig. 3, both horizontal and vertical emittances are being cooled at a comparable rate. Because the space-charge tune shift of proton bunches becomes significant during cooling, it may effect the proton beam lifetime. In such a case, one can introduce horizontal heating to control the space-charge tune shift and proton beam lifetime.

The design of the cooling section will closely follow the LEReC approach [13]. To maintain the transverse angle deviation of the electron beam trajectory $< 20 \mu\text{rad}$, the integral of residual transverse magnetic field between correctors in the cooling region must be kept below $1 \mu\text{Tm}$. Shielding of the residual magnetic field to such level will be achieved using concentric cylindrical layers of high-permeability alloy in the cooling sections [14]. Some cooling section space will be taken up by short (0.2 m) weak solenoids, which control the angular spread of the electron beam due to its space charge. Such solenoids will be placed approximately every 10 m along the cooling section.

The main parameters of the electron cooler are listed in Table I. Here, we assumed a cooling section length of 130 m. Once engineering layout starts, electron cooler parameters, such as hadron beam beta-functions in the cooling section and length of the cooling section, can be adjusted as necessary.

TABLE I. Parameters of an electron cooler for 23.8 GeV proton beam energy.

| | |
|--|--------------------|
| Proton repetition rate | 24.6 MHz |
| RMS proton bunch length | 60 cm |
| Relativistic gamma | 25.4 |
| Proton energy | 23.8 GeV |
| Electron energy | 13.0 MeV |
| Length of cooling section | 130 m |
| Proton beta function (minimum) in the cooling section | 150 m to 200 m |
| Single electron bunch charge | 2.5 nC |
| Total electron charge per proton bunch | 5 nC |
| Average electron current | 123 mA |
| RMS normalized emittance | 2.0 μm |
| RMS electron angular spread | 30 μrad |
| RMS electron energy spread | 5×10^{-4} |
| RMS electron bunch length | 5 cm |

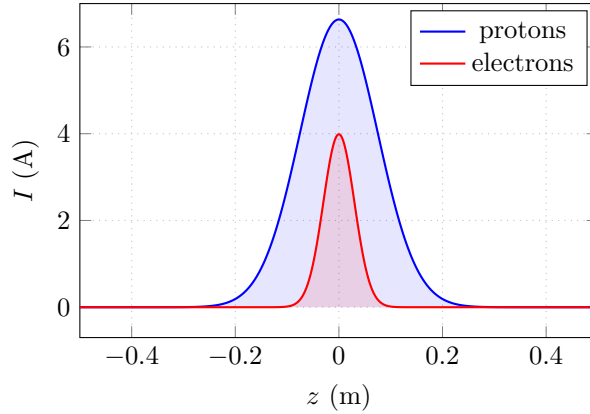


FIG. 4. Time structure of a single electron bunch synchronized with a single proton bunch for cooling at 41 GeV.

IV. ELECTRON COOLER PARAMETERS FOR COOLING PROTONS AT 41 GeV BEAM ENERGY

The role of the electron cooler at 41 GeV is to counteract IBS with a growth time of 2 hours and to maintain beam emittances close to their initial values. As result, the electron beam requirements are relaxed compared to those required for the pre-cooling

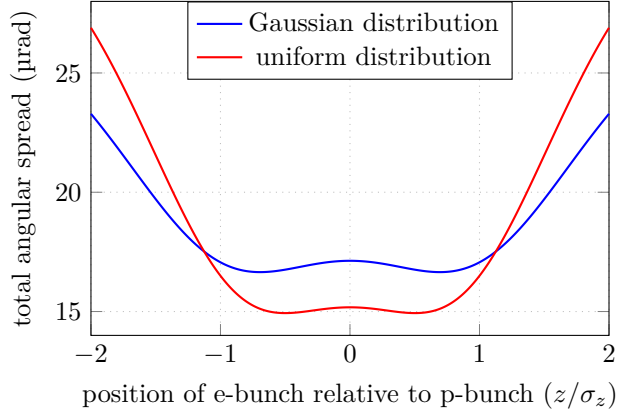


FIG. 5. Electron angles in the cooling section from beam emittance and proton space charge for cooling at 41 GeV for two possible electron bunch profiles.

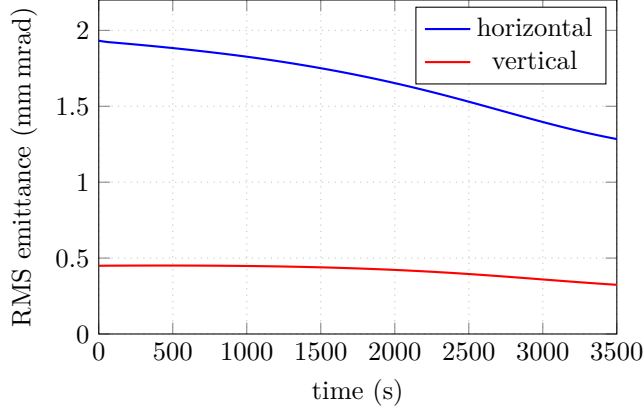


FIG. 6. RMS normalized emittance during cooling at 41 GeV using a single electron bunch placed in the middle of the proton bunch.

at 23.8 GeV.

At 41 GeV, the length of a proton bunch is 7.5 cm RMS, and the repetition frequency is 98.5 MHz. At this energy, one electron bunch from an electron accelerator will be synchronized with one proton bunch as shown in Fig. 4.

In simulations, we assumed the total angular spread of the electrons in the cooling section to be 20 microradians. The contributions to the angles in the cooling section from the electron beam emittance and the space charge of the proton beam are shown in Fig. 5. The results of cooling simulations with a single electron bunch per proton bunch and

parameters from Table II are shown in Fig. 6. One can see that emittance growth due to IBS is fully counteracted by cooling and emittances are maintained close to their initial values. The initial emittances assume that the vertical emittance of the protons was already pre-cooled at the proton injection energy.

TABLE II. Parameters of an electron cooler for 41 GeV proton beam energy.

| | |
|--|--------------------|
| Proton repetition rate | 98.5 MHz |
| RMS proton bunch length | 7.5 cm |
| Relativistic gamma | 43.7 |
| Proton energy | 41 GeV |
| Electron energy | 22.3 MeV |
| Length of cooling section | 130 m |
| Proton beta function (minimum) in the cooling section | 150 m to 200 m |
| Electron charge per proton bunch | 1.0 nC |
| Average electron current | 99 mA |
| RMS normalized electron emittance | 2.0 μm |
| RMS electron angular spread | 20 μrad |
| RMS electron energy spread | 5×10^{-4} |
| RMS electron bunch length | 3 cm |

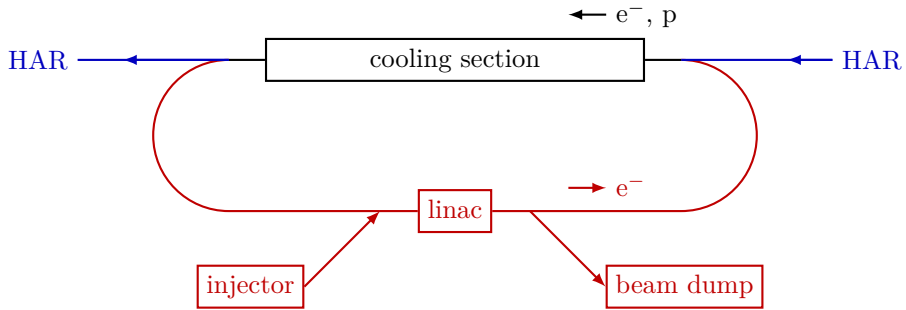


FIG. 7. Schematic layout of the electron cooler.

V. OVERVIEW OF THE ELECTRON ACCELERATOR

A. Accelerator layout

The electron cooler layout, shown schematically in Fig. 7, consists of an injector with a HVDC photoemission gun operating at 400 keV followed by QWR 197 MHz SRF cavities, the SRF Linac, an electron beam transport line from the SRF linac to the cooling section, the cooling section, the return beam line, and a high-power beam dump.

B. Injector Optimization

Reference simulations of the injector and electron linac were performed using the code PARMELA, which showed that the required electron beam parameters could be achieved.

A second simulation study is under way to further optimize initial results using the 3D space charge code General Particle Tracer (GPT), and identify any possible beneficial modifications to the injector layout using Multi-Objective Genetic Algorithm Optimization (MOGA).

So far, the three injector layouts shown in Figure 8 have been studied. The first, labeled ‘v1’, duplicates the reference design simulated in PARMELA. Here particles are created in the LEReC-style 400 kV dc photogun using a cathode with mean transverse energy of 150 meV, typical for modern multi-alkali cathodes. The beam then proceeds through two emittance compensating solenoids to two 197 MHz quarter-wave cavities. This approach relies on the longitudinal space charge forces to stretch the initial pulse to the desired 5 cm RMS bunch length before being accelerated to several MeV in these cavities. The beam is then sent through a 591 MHz cavity to remove residual RF curvature before being sent through a merging system into the main linac. The second layout takes a similar approach but moves the first accelerating cavity closer to the gun (in between the two solenoids), thereby limiting the distance the beam travels at the lowest energy and possibly mitigating negative effects of the space charge on the energy spread and emittance. The third layout replaces the accelerating cavity between the solenoids with a cavity intended for bunching the beam, allowing for longer initial pulses, and therefore smaller transverse beam sizes and thermal emittances.

For the initial optimization of these layouts, the gun voltage was fixed at 400 kV and the laser shape set to be uniform both transversely and longitudinally. The transverse and longitudinal laser sizes were allowed to vary, as were the solenoid settings and cavity voltages and phases. Optimizations were carried out with a low number of macroparticles (2k), since the MOGA approach requires many thousands of simulations

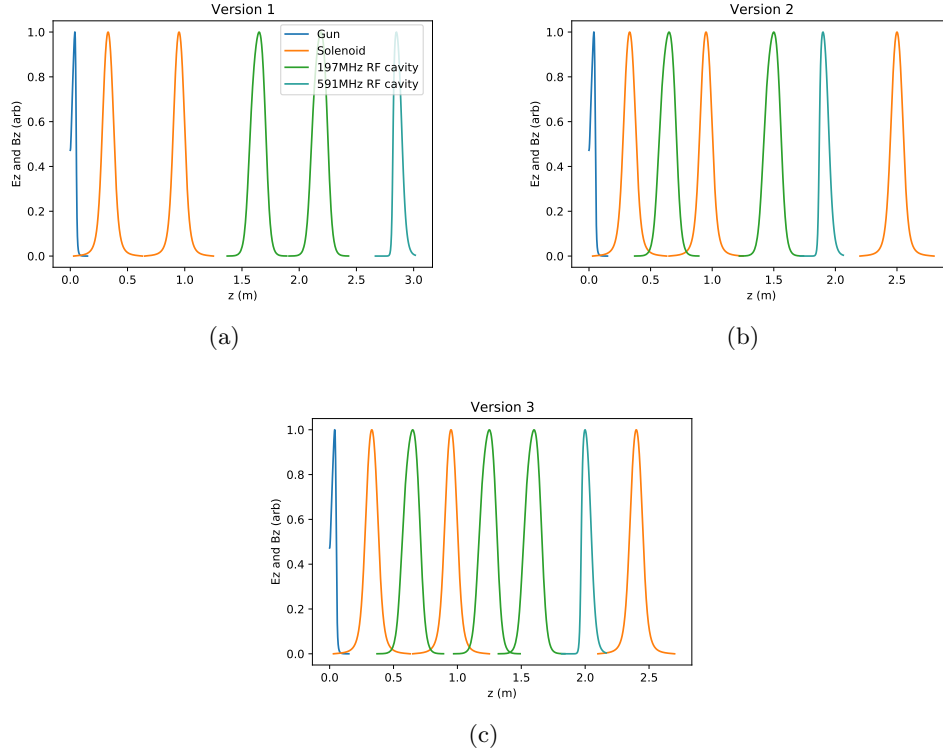


FIG. 8. Injector layouts for optimization. (a) shows the reference injector layout studied with PARMELA, while (b) and (c) give two possible alternatives.

to be performed. Individual optimal solutions are then examined using 100k particles. Testing for convergence of the resulting solutions by increasing macroparticles indicates that one can expect about 20% to 50% reduction in emittance values when switching from 2k to 100k macroparticles, while the energy spread remains essentially the same. Figure 9 shows the resulting optimal emittance vs. energy spread curves for the three layouts after optimizing for 80 generations with 800 individuals per generation.

Pulling individual solutions near the turnover point in each front shows that the slice emittance along the bunch at the end of each injector is roughly the same, as seen in Fig. 10. This implies the improved emittance performance seen in the optimal fronts arises from the ability to align the individual slice emittances at a particular screen location. Note that the beginning of the cooling section is the real location of interest for aligning the slices of the beam. From this one concludes that the injector reference design will perform as well as the other layouts once the optimization is complete.

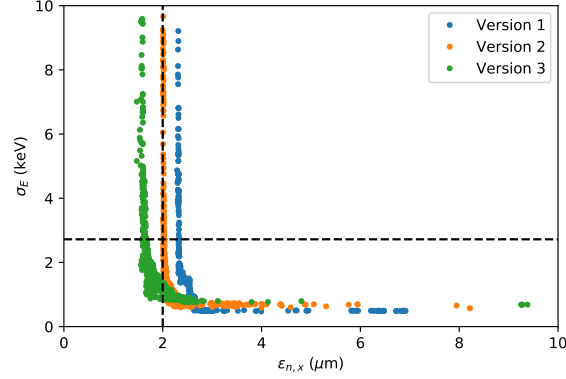


FIG. 9. Optimized emittance vs. energy spread for the three injector layouts.

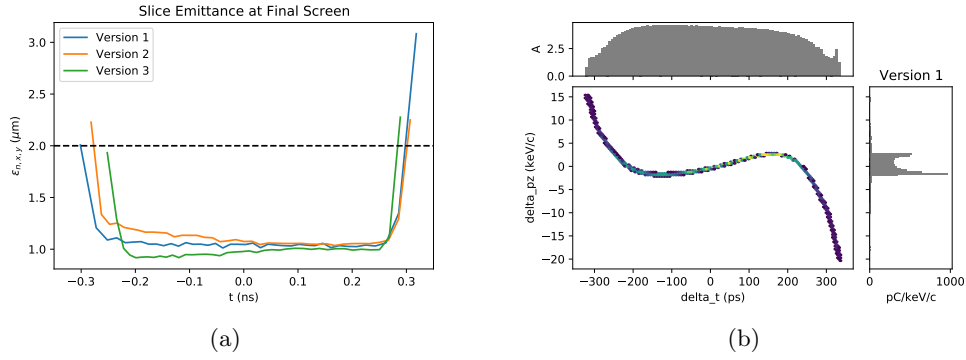


FIG. 10. (a) slice emittance along bunch at the final screen for each layout (b) longitudinal phase space for baseline layout at final screen.

C. Electron beam linac simulations

Baseline simulations of the linac were performed using the code PARMELA to ensure that the electron beam parameters required for cooling could be preserved during acceleration and beam transport. Simulations were performed for three different lengths of electron bunches on the cathodes and showed that, in all three cases, the required electron beam parameters, listed in Table I, could be achieved. Simulations also show that a shorter electron pulse length on the cathode of 350 ps is preferred since it results in a smaller energy spread.

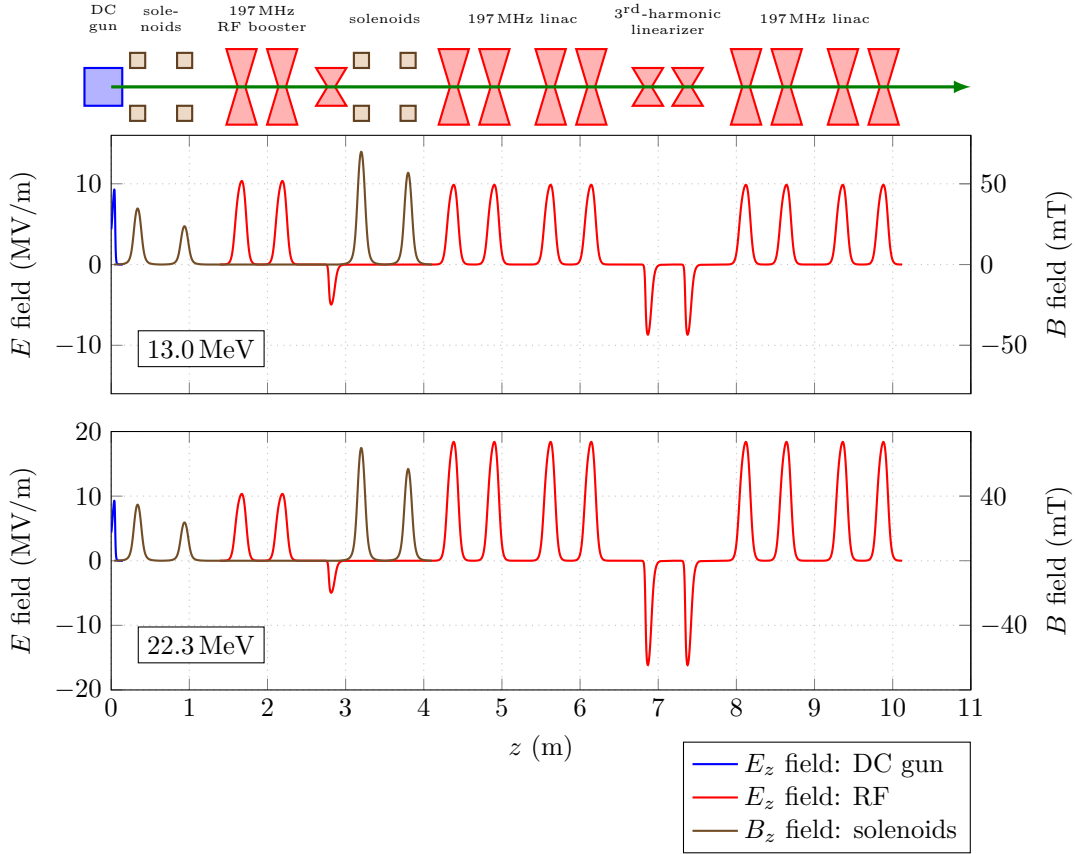


FIG. 11. Linac layout and fields for the 13.0 MeV (top) and 22.3 MeV (bottom) electron accelerator.

The linac layout and fields are shown in Fig. 11. Figure 12 shows the resulting beam emittances and energy spread at the end of the linac in both the 13.0 MeV case for pre-cooling of protons at 23.8 GeV and the 22.3 MeV case for cooling at 41 GeV, the latter satisfying the parameters listed in Table II.

D. ERL Physical Layout

The physical cooler ERL layout is shown in Fig. 13. In this layout, the linac (shown in green) is placed in the IR2 hall and the beam transported away from IR2 to a 180 deg turn around (right side), co-propagated with the proton beam for 130 meters, turned around again and transported back to the linac for energy recovery. The benefit of

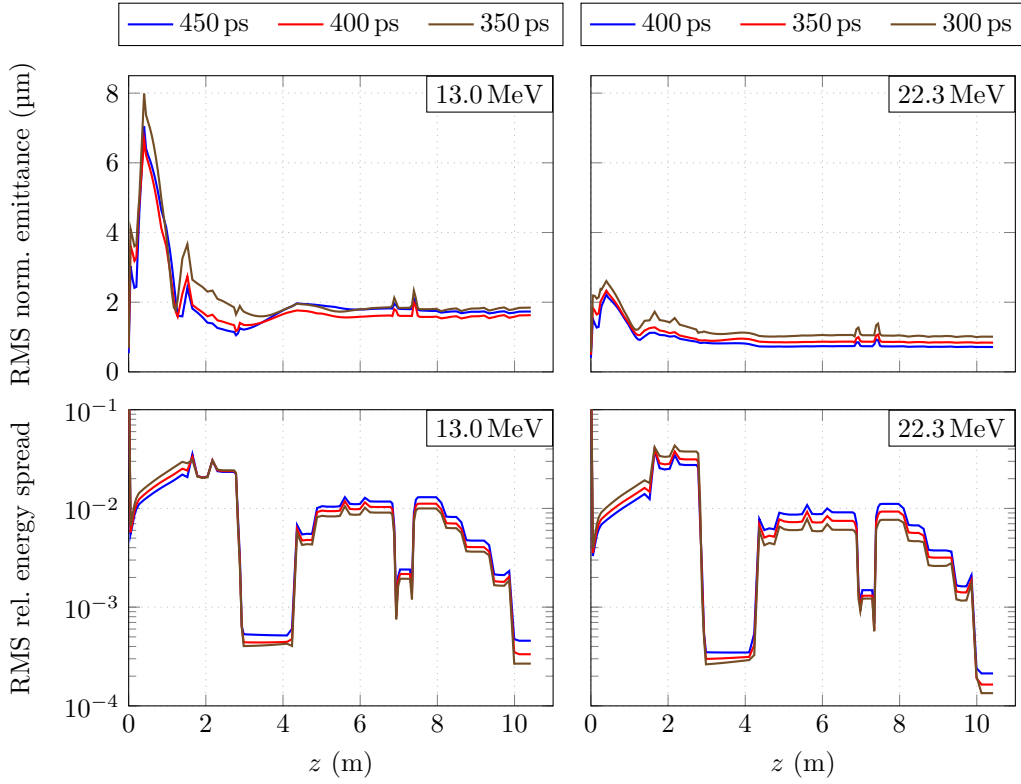


FIG. 12. Emittance and energy spread at the end of the electron linac for three different electron bunch lengths at the cathode. Left: 13.0 MeV, right: 22.3 MeV. The charge is 2.5 nC for the 13.0 MeV case and 1.0 nC for the 22.3 MeV case.

this approach is the placement of the injector, linac, merger, and beam stop in the IR2 hall.

Design of the turnaround in such a layout will need careful thought. One possible solution that allows for a closed dispersion after the turnaround is shown in Fig. 14.

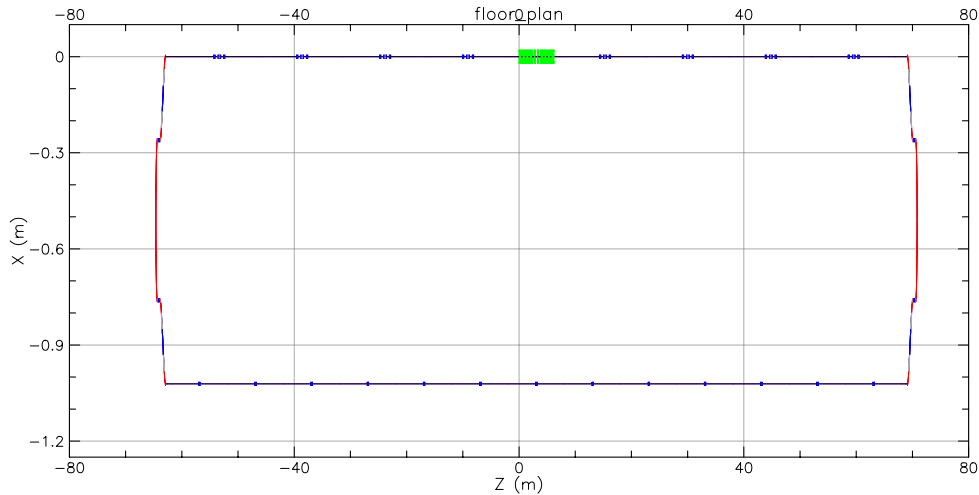


FIG. 13. Basic ERL layout in Bmad with symmetric placement of the linac in the IR2 hall. Note that the vertical and horizontal scales are very different.

VI. ACCELERATOR SYSTEMS

A. Injector

1. Photocathode

The electron beam will be generated by a laser illuminating an alkali antimonide cathode such as K_2CsSb or Na_2KSb , which both show great promise towards meeting the goals of high average current and good lifetime. High quantum efficiency (QE) performance of the gun is obtained by fabricating the cathode on a clean substrate in a UHV environment, and transporting it to the injector through a UHV load-lock system.

Using $E_{\text{cath}} = 4.5 \text{ MV m}^{-1}$ as typical for demonstrated high-voltage DC guns, and a mean transverse energy (MTE) of 0.3 eV as measured and simulated for K_2CsSb illuminated with 532 nm laser light, one finds that $1.6 \mu\text{m}$ RMS normalized emittance should be achievable for 2.5 nC per bunch operation with an optimum laser spot size.

To support long-term operation at high current, a special cathode storage system was developed at BNL, shown in Fig. 15. Such a vacuum suitcase is able to deliver 12 active cathodes at once. With the state-of-the-art cathode production and delivery system, as well as excellent cathode lifetime, it was possible to support continuous operation at high current for months during RHIC operation [15].

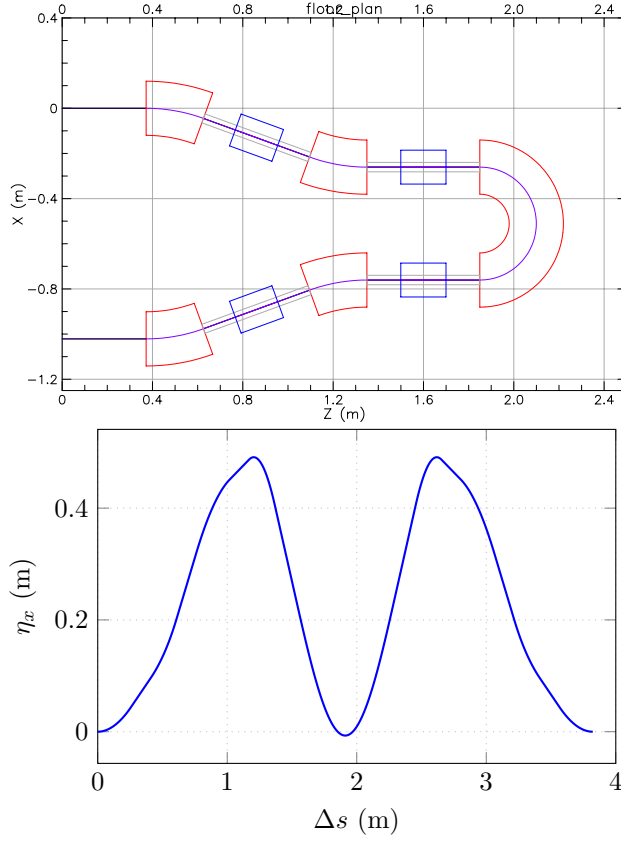


FIG. 14. Possible solution for the turnaround system that allows for closed dispersion.

2. HVDC Gun

For the electron injector, we assume a LEReC type HVDC gun as the electron source. BNL has good experience with high-current electron beam operation [10].

Fig. 16 shows the LEReC HVDC gun model. A gap voltage of 400 kV has been demonstrated, with continuous stable operation. At this voltage, the gradient on the cathode surface is 4.5 MV m^{-1} . We will have a 4 mm radius laser size, placed off-center by 6 mm to avoid ion back-bombardment. Biasing the anode and using ion clearing electrodes will help to eliminate the ions from the downstream beamline. Trim coils are used to move the beam back to the beam line center. A solenoid is placed 30 cm away from the photocathode.

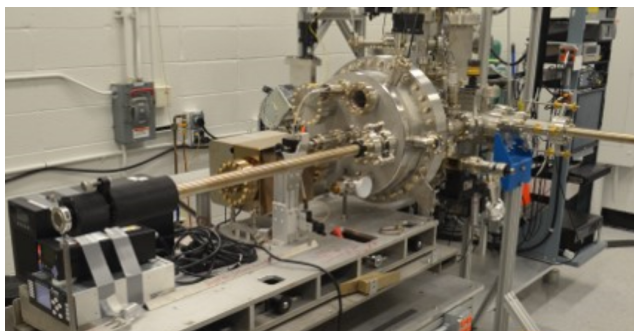


FIG. 15. LEReC vacuum suitcase capable of holding 12 active cathodes.

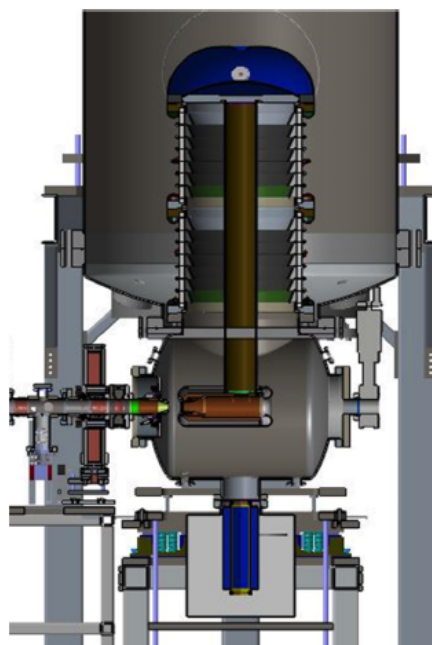


FIG. 16. LEReC HVDC gun cross section view. Beam travels to the left.

B. RF considerations

Both the ERL and the injector booster use 197 MHz SRF cavities for acceleration and 591 MHz 3rd-harmonic cavities to create a flat top of the waveform. Small changes in the phase and amplitude of the 591 MHz cavities can be used to compensate for linear slopes or quartic distortions in the longitudinal phase space. The ESR/HSR 591 MHz

cavity shape can be used for the ERL 3rd-harmonic cavity design, with changes in the end group configuration. The ESR/HSR cavities chose a low R/Q elliptical design to mitigate the transient beam loading in the storage rings and compromised some other specifications, which is not necessary in the ERL. However, the compromised specifications are still adequate for the ERL cavities.

To keep the 197 MHz cavity reasonably small in size to fit into the modular cryostats and the cavity fabrication/processing/testing facilities, a longitudinal QWR design is adopted. The transverse diameter of this cavity is expected to be slightly larger than the 591 MHz storage ring cavities and smaller than the 197 MHz crab cavity designs. The cavity shape is being optimized for maximum acceleration voltage with constraints on cavity size and peak surface field. The surface and cross-section field of the cavity's fundamental mode is shown in Fig. 17. Table III shows the parameters of the fundamental and harmonic cavities in both the linac and the booster. Figures 18 and 19 show the conceptual fundamental cavity cryomodule designs for both the booster and the linac. The maximum beam power in the booster cavity is about 210 kW, which may require two coaxial fundamental power couplers. The beam power in the ERL is minimal, and a few kW of RF power is sufficient for each cavity. The ESR/HSR cavity beampipe HOM absorber design can be reused in the QWR cavity to satisfy the damping requirement of ~ 125 mA beam current, with minimal additional R&D effort.

In order to cool the 23.8 GeV protons during the accumulation stage of the HAR, and then cool the protons after ramping to up to 41 GeV, the frequency of the linac needs to be changed from 196.90 MHz to 197.00 MHz, a 102 kHz change after the HAR ramp. Such a tuning can be achieved with about 0.2 mm change in the cavity length, which is within the capability of traditional tuner design, even with additional range added for other tuning needs.

TABLE III. Basic parameters of the SRF cavities in the cooler ERL.

| | Booster fundamental | Main linac fundamental | Booster 3 rd harmonic | Main linac 3 rd harmonic |
|---|------------------------|---------------------------|-------------------------------------|--|
| Number of cavities | 1 | 8 | 1 | 1 |
| Cavity voltage (MV) | 1.7 | 2.9 | 0.43 | 2.6 |
| $R/Q = V^2/P_C$ (Ω) | 135 | 135 | 73 | 73 |
| Geometry factor G (Ω) | 83 | 83 | 284 | 284 |
| E_{peak} (MV m ⁻¹) | 27 | 46 | 2 | 28 |
| B_{peak} (mT) | 47 | 79 | 4 | 53 |

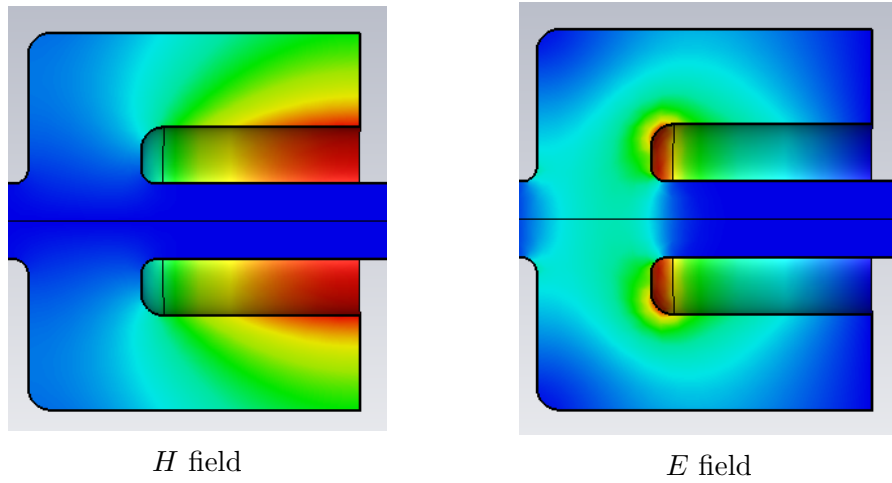


FIG. 17. Surface/cross-section magnetic and electric field in the 197MHz QWR cavity.

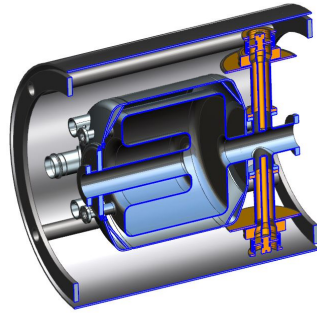


FIG. 18. Modular cryostat concept of the ERL booster 197MHz QWR cavity.

C. High-power beam dump

After energy recovery, the electron beam will be delivered to the high-power beam dump. An example of such a beam dump is shown in Fig. 20. The beam dump beamline must provide sufficient spreading of the high-power electron beam within the dump to reduce the current density to acceptable levels, and will need to be designed.

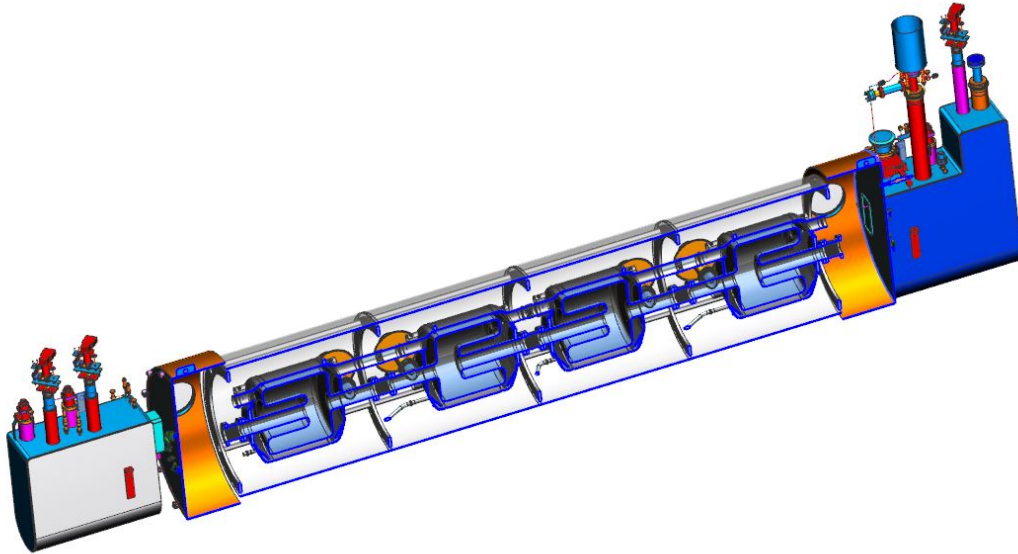


FIG. 19. 197 MHz cavities in the ERL cryostat.

D. Diagnostics

Plans for the diagnostics are based on the commissioning and operational experience of the LEReC cooler.

The main diagnostics systems guaranteeing a proper quality of the electron beam in the cooling section (CS) include: the longitudinal phase space diagnostic (LPSD) beamline, the emittance measurement stations, the beam position monitors (BPMs) and trajectory feedback, the spectrometer, and the energy feedback system.

The dedicated longitudinal phase space diagnostic beamline consists of a bending magnet creating horizontal dispersion on the profile monitor (PM) at the end of the beamline and the vertical deflecting cavity creating the correlation between the longitudinal position of the bunch slice and its vertical projection on the PM. Similar to the LEReC LPSD beamline [16], a dispersion of about 1 m will be required on the PM. The 50 μm resolution of the PM converts to a 5×10^{-5} resolution of $\Delta p/p$ measurement along the electron bunch. The voltage requirement for the deflecting cavity is a subject of optimization of the LPSD beamline parameters. For example, limiting the beamline length to 5 m and requesting 2 ps longitudinal resolution, we end up with a 70 kV requirement on the cavity amplitude for a 197 MHz deflecting cavity.

The beam emittance must be measured at the entrance and the exit of the cooling



FIG. 20. Example of the LEReC high-power beam dump.

section. Both the moving slit and the multi-slit emittance measurement setups provide good results (see [9] for example). Each emittance measurement station consists of the horizontal/vertical moving slit combo and the PM located downstream of the slit. Long CS drifts provide a perfectly adequate space between the slit and the PM to achieve the proper measurement resolution.

The CS BPMs equipped with the custom VME-based V301 electronics modules [17] can be installed every ten meters. The properly shielded cooling section guarantees that the BPM-to-BPM regions can be treated as true field-free drifts. Hence, the algorithm of alignment of electron-ion trajectories [18], successfully implemented at the LEReC, can be employed for the EIC coolers. Requesting a $15 \mu\text{rad}$ RMS angle for the electron-ion trajectory alignment, we end up with a $100 \mu\text{m}$ tolerance on the accuracy of BPM readings. Such an accuracy can be consistently achieved with the aid of the BPM switching modules [19, 20]. The LEReC experience also points to a necessity of having trajectory feedback systems — both a fast and a slow one. The slow feedback system, compensating trajectory drift, can be based on regular slow correctors, which are the integral part of the CS solenoid-corrector modules. The fast feedback must be capable of providing a few kHz response and will require a set of dedicated fast correctors. The feedback can employ a simple mathematical algorithm outlined in [21].

Precise matching of the electron and the hadron beam γ -factors will require a high accuracy spectrometer [22]. A well mapped bending magnet [23], which could be part of the 180 degree bend in Figure 14, is the best candidate for such a spectrometer. A

dedicated recombination monitor (see [22] for details) can be considered as an auxiliary γ -matching diagnostics device. The same spectrometer that is utilized for the matching of the beams γ -factors will be used for the energy feedback, which must counteract the slow drift of electron beam energy.

VII. CONCLUSIONS

A feasibility study of an electron cooler for pre-cooling of protons at injection energy of 23.8 GeV and cooling at 41 GeV was performed. No showstoppers for designing such an electron cooler were found. Simulations of an electron beam injector using a LEReC-type DC photoemission gun were performed, and the required electron beam parameters were obtained. Simulations of the electron linac also showed that the electron beam parameters required for cooling are achievable. More detailed simulations and design studies of the electron accelerator will follow.

-
- [1] Electron-Ion Collider at Brookhaven National Laboratory, Conceptual Design Report, 2021.
 - [2] G.I. Budker, *Atomnaya Energia*, V.22, p. 346 (1967).
 - [3] Frequent On-Energy Injection Design Option of Electron-Ion Collider, BNL Technical Note BNL-220687-2020-TECH, 2020.
 - [4] A. V. Fedotov et al., Experimental demonstration of hadron beam cooling using radio-frequency accelerated electron bunches, *Phys. Rev. Letters* 124, 084801 (2020).
 - [5] Ya. Derbenev, A. Skrinsky, *Part. Acc.* 8 (1978), p. 235; *Sov. Phys. Rev* 1 (1981), p. 165.
 - [6] H. Poth, *Physics Reports* 196, Nos. 3 and 4, pp. 135-297 (1990).
 - [7] S. Nagaitsev et al., *Phys. Rev. Lett.* 96, 044801 (2006).
 - [8] S. Chandrasekhar, *Principles of Stellar Dynamics* (U. Chicago Press, 1942).
 - [9] D. Kayran et al., High-brightness electron beams for linac-based bunched beam electron cooling, *Phys. Rev. Accel. Beams* 23, 021003 (2020).
 - [10] X. Gu et al., Stable operation of a high-voltage high-current dc photoemission gun for the bunched beam electron cooler in RHIC, *Phys. Rev. Accel. Beams* 23, 013401 (2020).
 - [11] S. Seletskiy and D. Kayran, Requirements to the cooling section solenoidal field in the EIC low energy cooler, BNL Tech Note, BNL-216176-2020-TECH, April 9 2020.
 - [12] S. Seletskiy, Effect of hadron-electron focusing in EIC low energy coolers, BNL Tech Note, BNL-216178-2020-TECH, May 7 2020.
 - [13] A. Fedotov et al., in *Proc. North American Particle Accelerator Conf. (NAPAC'16)*, Chicago, IL, USA, Oct. 2016, pp. 867-869.
 - [14] S. Seletskiy et al., in *Proc. North American Particle Accelerator Conf. (NAPAC'16)*, Chicago, IL, USA, Oct. 2016, pp. 1030-1032.
 - [15] E. Wang et al., in *Proc. of IPAC2019 (Melbourne, Australia, 2019)*, p. 2154.

- [16] T.A. Miller et al., LEReC Instrumentation Design and Construction, in Proc. 5th Int. Beam Instrumentation Conf. (IBIC'16), Barcelona, Spain, Sep. 2016.
- [17] Z. Sorrell, P. Cerniglia, R. Hulsart, R. Michnoff, Beam Position Monitors for LEReC, in Proc. 5th Int. Beam Instrumentation Conf. (IBIC'16), Barcelona, Spain, Sep. 2016.
- [18] S. Seletskiy et al., Alignment of Electron and Ion Beam Trajectories in Non-Magnetized Electron Cooler, in Proc. 8th Int. Particle Accelerator Conf. (IPAC'17), Copenhagen, Denmark, May 2017.
- [19] Z. Sorrell, P. Cerniglia, R. Hulsart, K. Mernick, R. Michnoff, Beam position monitors for LEReC, Report No. BNL-112674-2016-CP, BNL (2016).
- [20] R. Hulsart, R. Michnoff, P. Thieberger, S. Seletskiy, Some considerations about switching BPM channels, Report No. BNL-213694-2020-TECH, BNL (2020).
- [21] S. Seletskiy et al., Achieving and optimizing transverse cooling in the first non-magnetized bunched electron cooler, to be published.
- [22] S. Seletskiy et al., Accurate setting of electron energy for demonstration of first hadron beam cooling with rf-accelerated electron bunches, Phys. Rev. Accel. Beams 22, 111004 (2019).
- [23] H. Song et al., High-precision magnetic field measurement and mapping of the LEReC 180° bending magnet using very low field NMR with Hall combined probe, Meas. Sci. Technol. 31 075104, (2020).